Journal of Fluids and Structures 78 (2018) 52–68

Contents lists available at ScienceDirect

Journal of Fluids and Structures

journal homepage: www.elsevier.com/locate/jfs

A fully-coupled generalized model for multi-directional wind loads on tall buildings: A development of the quasi-steady theory

Wei Cui, Luca Caracoglia *

Department of Civil and Environmental Engineering, Northeastern University, Boston, MA, 02115, USA

HIGHLIGHTS

- A new generalized dimensionless approach for tall building aerodynamics is proposed.
- Inter-modal coupling due to fluid–structure interaction is explicitly analyzed.
- Wind tunnel HFFB results are incorporated into a generalized aerodynamic formula.

ARTICLE INFO

Article history:
Received 29 April 2017
Received in revised form 25 November 2017
Accepted 6 December 2017
Available online 4 February 2018

Keywords:
Line-like structures
Quasi-steady aerodynamic theory
Tall buildings
Coupled modes
3D effects
Analytical formulation

ABSTRACT

This study examines in detail the quasi-steady aerodynamic theory, which is widely applied in wind engineering for the evaluation of wind loads. The authors propose an alternative approach and a novel generalized aerodynamic formulation for the wind-induced dynamic response of a bluff body. The proposed formulation is applied to the dynamic analysis of tall buildings, considering multi-directional wind loads, aerodynamic damping and aerodynamic stiffness effects, and inter-modal structural coupling. Dimensionless Fourier transformation is used in the formulation to provide a general "unified formula" and new insights on the modeling and estimation of wind loads. One numerical example is presented to verify the validity of the formula; numerical simulations are compared against literature data (wind tunnel test results) for a benchmark building structure.

1. Introduction

1.1. Foreword: advantages and limitations of the quasi-steady aerodynamic theory for the analysis of wind loads on vertical slender structures

The quasi-steady aerodynamic theory plays a fundamental role in the examination of wind loads, since the early stages of wind engineering research and the pioneering work by Professor Davenport (Davenport, 1961). In his original contribution, Professor Davenport demonstrated that the wind-induced structural response can be determined in the frequency domain by combining local wind climatology, local wind exposure (influenced by terrain roughness and topography), structural aerodynamic characteristics (governed by building shape) and structural dynamic properties (mass and stiffness distribution and damping ratios). The main steps of this approach are summarized by the Davenport Chain, which is illustrated in Fig. 1. This original idea has been employed in both wind engineering research and practice for several decades.

* Correspondence to: Department of Civil and Environmental Engineering, Northeastern University, 400 Snell Engineering Center, 360 Huntington Avenue, Boston, MA 02115, USA.
E-mail address: lucac@coe.neu.edu (L. Caracoglia).

https://doi.org/10.1016/j.jfluidstructs.2017.12.008
0889-9746/

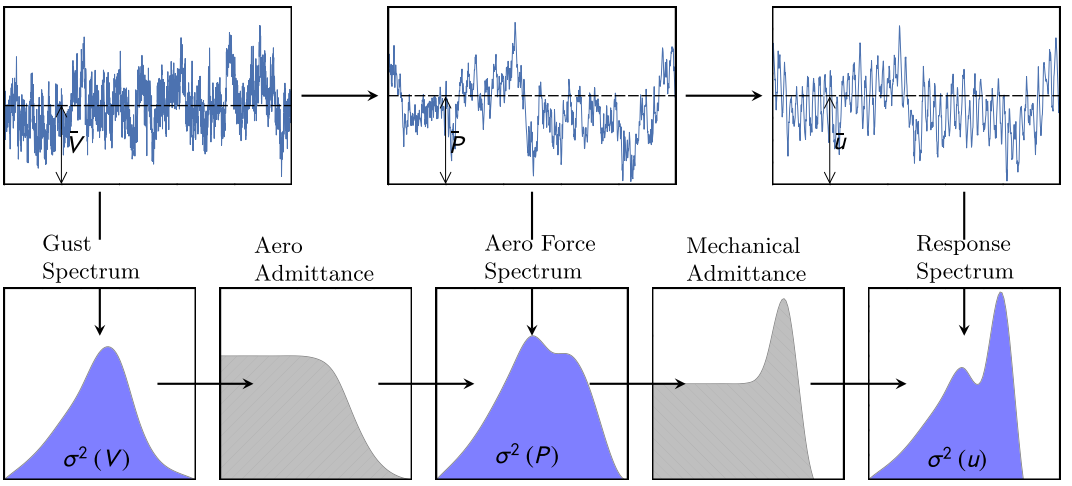

Fig. 1. Davenport Chain (Isyumov, 2012).

The original formulation was conceived to examine wind loads by focusing on a single (constant) wind direction at a time. Several authors have contributed to the further advancement of this theory for vertical slender structures such as tall buildings (e.g., Solari, 1993a,b; Piccardo and Solari, 1998a).

Because of the increasing slenderness and irregular shape in modern buildings, the approach for evaluation of wind loads has been significantly revised. For example Chen and Kareem (2005), exploiting theoretical derivations of the quasi-steady theory, proposed a general solution to evaluate the dynamic response of tall buildings by considering non-uniplanar mode shapes and inter-modal coupling. Piccardo and Solari (1998a, 2000) advanced a generalized formulation to evaluate the along-wind, cross-wind and torsional response of slender structures. In the presence of an irregular building shape, the eccentricity between mass and rigidity centers cannot be ignored. This eccentricity leads to structural coupling between lateral translation motion and rotation about the vertical building axis, first examined by Kareem (1985). Attention towards wind load analysis, accounting for a fully three-dimensional (3D) structural modeling, has been recently noted. For example, He and Macdonald (2016) proposed a method to examine generalized three-degree-of-freedom galloping instability of slender vertical structures through the extension of the quasi-steady theory, which is a derivation from a 2D model by Nguyen et al. (2015) considering the coupling between drag and lift forces for buffeting and aeroelastic response.

Finally, multi-directional wind load analysis, coupled with modal expansion with nonlinear mode shape functions, is often desirable in the presence of complex and unconventional buildings with large slenderness ratios, which often represent the modern architectural design trend. All the above aspects have been separately considered by most researchers; a generalized aerodynamic theory is still possibly needed for the design of future buildings.

1.2. Relevance of the quasi-steady theory in the context of performance-based wind engineering

Performance-based engineering is a well established probabilistic design methodology, routinely applied by structural engineers in seismic engineering (SEAOC, 1995). The basic idea is to ensure that a structure, subjected to different hazard levels, satisfies a set of minimum performance requirements (e.g., Inokuma, 2002). This methodology is a substantial evolution from the prescriptive structural design since it ensures that life safety and collapse prevention are preserved in the case of an extremely severe hazard, and occupancy disruptions are minimized in other cases.

In recent years, similar concepts have been put forward to derive a "basic theory" for performance-based wind engineering (PBWE) (Ciampoli et al., 2011; Ciampoli and Petrini, 2012). This topic has received much attention from the wind engineering community. The study by Smith and Caracoglia (2011) is among the first systematic implementations of PBWE to examine the wind-induced response of prismatic tall buildings; the quasi-steady aerodynamic theory was exploited to determine wind loads; the wind direction perpendicular to one of the vertical faces was only considered (as the most critical) and coupling of the structural modes was not examined (Smith and Caracoglia, 2011). Other examples include frameworks for the analysis of wind load variability (e.g., Bashor and Kareem, 2007; Chuang and Spence, 2017), a number of alternative methodologies for linear elastic building design (e.g., Norton et al., 2008; Jain et al., 2001; Spence and Kareem, 2014) and nonlinear inelastic structural response (Hart and Jain, 2013). In the case of wind load effects on low-rise buildings, structural failures can be related to capacity loss in key members or connections (Ellingwood et al., 2004; Ellingwood and Tekie, 1999).

Nevertheless, derivation of a possibly general (and practical) approach for PBWE, capable of investigating several performance objectives and limit states is not completely available, especially in the case of slender vertical structures such as tall buildings. As an essential part of PBWE, suitable formulas are desirable to calculate wind loads and structural response for variable wind speeds and directions. A unified formulation is consequently advantageous for a more systematic implementation of the PBWE.

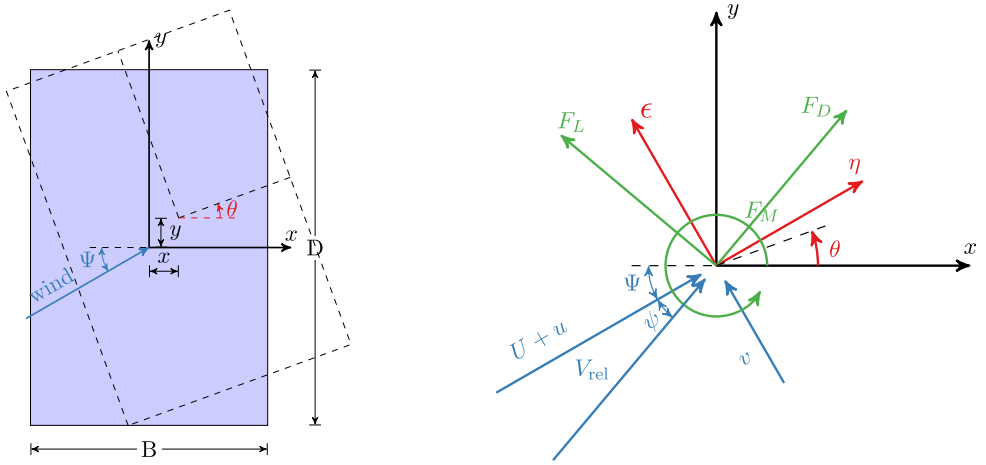

(a) Cross-sectional view of building at height z and schematic representation of 3D motion.

(b) 3D motion coordinates (detail).

Fig. 2. 3D motion coordinates and wind–pressure force vector representation.

1.3. Study objectives and purpose

This study proposes an alternative formulation that combines the effects of wind speed and wind direction into a unifying and "compact formula" for the analysis of wind loads on tall buildings, which can be easily adapted to study various load scenarios and multiple wind directions (in contrast with most existing calculation methods). The formulation builds on a series of extensions of the quasi-steady aerodynamic theory; it promotes the analysis of the dynamic response of a line-like vertical structure with coupled structural modes and inter-modal interaction, triggered by aerodynamic damping and aerodynamic stiffness effects. The formulation consequently enables a more general examination of 3D aerodynamics and coupled-mode structures. In the formulation of the unified model, the loss of correlation in the wind loads along the principal vertical axis is exclusively considered. Even though extended models are available to examine the effects of the loss of correlation in both vertical (length-wise) and horizontal ("chord-wise") directions (e.g., Solari, 1993a,b) the proposed approach is still adequate and retains sufficient simplicity as to enable subsequent application to PBWE. The effects of wake-induced loading due to vortex shedding (along with the relevance of signature turbulence vs. incoming turbulence effects) are indirectly taken into account in the last part of the study by suitable "correction" of the proposed generalized quasi-steady formulation and by using information derived from wind tunnel experiments on a rigid model of a tall building (high-frequency force balance tests). Following the original work by Holmes (1987), the approach by Zhou et al. (2002) is used to calculate the generalized wind loads with wake-induced effects in the case of nonlinear mode shapes. Finally, even though the main focus of the study is on tall buildings, the formulation is expressed in dimensionless form to possibly enable application to other structures.

2. Formulation for 3D aerodynamics and coupled-mode structural dynamics

2.1. Dimensionless governing equation for the building motion in frequency domain

A tall building with mass and/or stiffness eccentricities may undergo complex motion under turbulent wind loads. The response of a tall building, and a slender structure in general, is characterized by non-negligible interaction between structural motion and flow and pressure field. Among the various contributions in the field of wind engineering and buildings aerodynamics, a number of key studies and results are used in this section. Further examination of these studies provided the motivation for this study and confirmed the initial renewed interest for this topic. Since the first implementation of Davenport Chain, it has been observed that the complex building aerodynamics and consequent dynamic response can be successfully resolved by accounting for all possible effects rather than introducing a number of simplifications, such as the limited influence of higher modes and modal coupling on the dynamics.

A fully 3D coupled-mode stochastic model is not currently available in general form, especially for PBWE applications. The existing model by Chen and Kareem (2005) accounts for inter-modal coupling by exploiting results from classical random vibration theory. However, it may not be fully suitable for the derivation of the wind-induced vibration of a tall building in a PBWE setting, due to the lack of correlation in the pressure loads (Cui and Caracoglia, 2015). The proposed alternative formulation is based on the representation of the wind load for a continuum structure, which is expressed as a combination

of drag force $F_D(z,t)$, transverse (or lift) force $F_L(z,t)$ and torque $F_M(z,t)$ per unit height. The forces per unit height can be appropriately found by projection of the drag and lift forces along the mean-wind direction angle Ψ and the principal horizontal local axes of the structure, schematically illustrated in Fig. 2(b); the derivation of the equations below (Eq. (1)) is inspired by the standard quasi-steady approach for line-like structures, for example described in Solari (1993a, b); Piccardo and Solari (2000). First-order effect are only retained in the formulation below, valid for small dynamic rotations about the angle Ψ and some lateral displacements.

$$F_D(z,t) = \frac{1}{2}\rho U^2(z)\,DC_D(\Psi) + \frac{1}{2}\rho U^2(z)\,DC_D'(\Psi)\,(\psi(t)-\theta(t)) + \rho DU(z)\,(u-\dot{\eta})C_D(\Psi) \tag{1a}$$

$$F_L(z,t) = \frac{1}{2}\rho U^2(z)\,DC_L(\Psi) + \frac{1}{2}\rho U^2(z)\,DC_L'(\Psi)\,(\psi(t)-\theta(t)) + \rho DU(z)\,(u-\dot{\eta})C_L(\Psi) \tag{1b}$$

$$F_M(z,t) = \frac{1}{2}\rho D^2\left[U^2(z) + 2U(z)\,(u-\dot{\eta})\right]\left[C_M(\Psi) + C_M'(\Psi)\,(\psi(t)-\theta(t))\right] \tag{1c}$$

In Eq. (1) $U(z)$ is the mean wind velocity, measured along the building height (coordinate z) and u is the zero-mean along-wind turbulence component relative to $U(z)$. The quantity $\dot{\eta}$ is the building translation speed component in the along-wind direction; ρ is the air density, D is a reference building width.

The quantity Ψ is the mean-wind attack angle and $\psi(t)$ is the instantaneous dynamic attack angle relative to Ψ. The angle $\psi(t)$ can be calculated as $\psi(t) = (v-\dot{\epsilon})/U(z)$, where v is the cross-wind turbulence component and $\dot{\epsilon}$ is the building translation speed component in the cross-wind direction. The angle $\theta(t)$ measures the instantaneous rotation of the building cross section and also depends on z; D is the structure's reference width, shown in Fig. 2(a). The aerodynamic coefficients $C_D(\Psi)$, $C_L(\Psi)$ and $C_M(\Psi)$ are drag and lift forces and torque measured at mean-wind incidence angle Ψ; $C_D'(\Psi)$, $C_L'(\Psi)$ and $C_M'(\Psi)$ are their derivatives with respect to the attack angle, evaluated at mean-wind incidence angle Ψ. The previous equations are strictly valid for "compact" cross section, in which the characteristic dimensions of the structure on the horizontal plane, B and D, have similar values. In the case of an elongated cross-sectional shape with large side ratio B/D, i.e. a bridge deck (Scanlan and Jones, 1990) or a system where the aerodynamic center and the geometric center are distant from each other, the coupling should account for supplementary terms to more correctly simulate aeroelastic interaction.

From classical structural dynamic theory, the governing equation of a continuum structure is

$$\mathbf{M}(z)\,\ddot{\mathbf{d}} + \mathbf{C}(z)\,\dot{\mathbf{d}} + \mathbf{K}(z)\,\mathbf{d} = \overrightarrow{\mathbf{F}}(z,t) \tag{2}$$

in which $\mathbf{d}$ is the structural response and deformation vector $\mathbf{d} = \begin{bmatrix} x & y & \theta \end{bmatrix}^T$

The static force $\bar{\mathbf{F}}$ associated with the effect of the mean wind speed can be separated from the Eq. (1):

$$\bar{\mathbf{F}} = \begin{cases} \frac{1}{2}\rho U^2(z)\,DC_D(\Psi) \\ \frac{1}{2}\rho U^2(z)\,DC_L(\Psi) \\ \frac{1}{2}\rho U^2(z)\,D^2C_M(\Psi) \end{cases} \tag{3}$$

Because all items in the previous equations are independent of time t, the structural static (mean) deformation is $\bar{\mathbf{d}} = \bar{\mathbf{K}}^{-1}\bar{\mathbf{F}}$.

The structural motion of a continuum structure can be further simplified by decoupling time and position (elevation z) through modal expansion, i.e. as the summation of multiple modes with generalized dimensionless coordinates $\chi_j(t)$ (truncated at mode N). This expansion can be written as:

$$x(z,t) = D\sum_{j=1}^{N}\chi_j(t)\phi_{x,j}(z) \tag{4a}$$

$$y(z,t) = D\sum_{j=1}^{N}\chi_j(t)\phi_{y,j}(z) \tag{4b}$$

$$\theta(z,t) = \sum_{j=1}^{N}\chi_j(t)\phi_{\theta,j}(z) \tag{4c}$$

in which $\phi_{x,j}(z)$, $\phi_{y,j}(z)$ and $\phi_{\theta,j}(z)$ are dimensionless components of the jth mode in the lateral directions x and y, and the torsional rotation θ.

After excluding the time independent force in Eq. (1), the 3D aerodynamic force can be separated into three parts: (1) quasi-steady wind force which only depends on the effects of turbulence; (2) aerodynamic damping force effect due to the structural motion velocity; (3) aerodynamic stiffness force effect caused by structural displacement (dependent on the instantaneous rotation at each floor).

For the first part, the quasi-steady wind force vector in Eq. (1) can be projected along the x and y axes corresponding to the local coordinate system to get:

$$\mathbf{F_q} = \begin{cases} \rho DU(z)\, u\left[C_D \cos\Psi - C_L \sin\Psi\right] + \\ \frac{1}{2}\rho DU(z)\, v\left[C_D' \cos\Psi - C_L' \sin\Psi - C_M \sin\Psi - C_L \cos\Psi\right] \\ \rho DU(z)\, u\left[C_D \sin\Psi + C_L \cos\Psi\right] + \\ \frac{1}{2}\rho DU(z)\, v\left[C_D' \sin\Psi + C_L' \cos\Psi + C_M \cos\Psi - C_L \sin\Psi\right] \\ \rho D^2 U(z)\, u C_M + \frac{1}{2}\rho D^2 U(z)\, v C_M' \end{cases} \tag{5}$$

The previous equations can be re-written in the following matrix form:

$$\mathbf{F_q} = \frac{\rho DU^2 \Delta(z)}{2} \begin{bmatrix} \cos\Psi & -\sin\Psi & 0 \\ \sin\Psi & \cos\Psi & 0 \\ 0 & 0 & 1 \end{bmatrix} \begin{bmatrix} 2C_D(\Psi) & C_D'(\Psi) - C_L(\Psi) \\ 2C_L(\Psi) & C_L'(\Psi) + C_D(\Psi) \\ 2DC_M(\Psi) & DC_M'(\Psi) \end{bmatrix} \begin{Bmatrix} \frac{u}{U} \\ \frac{v}{U} \end{Bmatrix} \tag{6}$$

where $\Delta(z) = (z/h)^{\alpha_b}$, which is the power law function of the atmospheric boundary layer at the building site. The quantity $U(h) = U$ is the reference mean wind speed measured at the top-floor elevation $z = h$.

The decomposition of the generalized wind force corresponding to mode j is:

$$F_q^j = \begin{bmatrix} \phi_{x,j} D & \phi_{y,j} D & \phi_{\theta,j} \end{bmatrix} \mathbf{F_q} \tag{7}$$

In a similar way, the generalized aerodynamic damping force is

$$\mathbf{F_a} = -\begin{cases} \rho DU\dot{\eta}(z)\left[C_D \cos\Psi - C_L \sin\Psi\right] + \\ \frac{1}{2}\rho DU\dot{\epsilon}(z)\left[C_D' \cos\Psi - C_L' \sin\Psi - C_D \sin\Psi - C_L \cos\Psi\right] \\ \rho DU\dot{\eta}(z)\left[C_D \sin\Psi + C_L \cos\Psi\right] + \\ \frac{1}{2}\rho DU\dot{\epsilon}(z)\left[C_D' \sin\Psi + C_L' \cos\Psi + C_D \cos\Psi - C_L \sin\Psi\right] \\ \rho D^2 U\dot{\eta}(z)\, C_M + \frac{1}{2}\rho D^2 U\dot{\epsilon}(z)\, C_M' \end{cases} \tag{8}$$

The buildings motion ϵ and η can be re-projected onto the x–y local building coordinates using the following transformation matrix:

$$\begin{Bmatrix} \epsilon \\ \eta \end{Bmatrix} = \begin{bmatrix} \cos\Psi & \sin\Psi \\ -\sin\Psi & \cos\Psi \end{bmatrix} \begin{Bmatrix} x \\ y \end{Bmatrix} \tag{9}$$

Using the same modal decomposition method, the generalized aerodynamic damping force of the mode j is:

$$\begin{aligned} F_a^j = -\sum_{k=1}^{N} \frac{1}{2}\rho DU \int_0^h \Delta(z) \begin{bmatrix} D\phi_{x,j} & D\phi_{y,j} & \phi_{\theta,j} \end{bmatrix} \begin{bmatrix} \cos\Psi & -\sin\Psi & 0 \\ \sin\Psi & \cos\Psi & 0 \\ 0 & 0 & 1 \end{bmatrix} \\ \left[\begin{Bmatrix} 2C_D \\ 2C_L \\ 2DC_M \end{Bmatrix} \begin{bmatrix} \cos\Psi & \sin\Psi & 0 \end{bmatrix} + \begin{Bmatrix} C_D' - C_L \\ C_L' + C_D \\ DC_M' \end{Bmatrix} \begin{bmatrix} -\sin\Psi & \cos\Psi & 0 \end{bmatrix} \right] \\ \begin{Bmatrix} D\phi_{x,k} \\ D\phi_{y,k} \\ \phi_{\theta,k} \end{Bmatrix} \dot{\chi}_k(t)\mathrm{d}z \end{aligned} \tag{10}$$

The aerodynamic stiffness force and generalized aerodynamic stiffness force of mode j can be expressed in the same way as follows:

$$\mathbf{F_s} = -\begin{cases} \frac{1}{2}\rho DU^2\theta(z)\left[C_D'\cos\Psi - C_L'\sin\Psi - C_D\sin\Psi - C_L\cos\Psi\right] \\ \frac{1}{2}\rho DU^2\theta(z)\left[C_D'\sin\Psi + C_L'\cos\Psi + C_D\cos\Psi - C_L\sin\Psi\right] \\ \frac{1}{2}\rho D^2U^2\theta(z)C_M' \end{cases} \tag{11}$$

$$F_s^j = -\sum_{k=1}^{N}\frac{1}{2}\rho DU^2\int_0^h \Delta^2(z)\left[D\phi_{x,j}\ D\phi_{y,j}\ \phi_{\theta,j}\right]\begin{bmatrix}\cos\Psi & -\sin\Psi & 0\\ \sin\Psi & \cos\Psi & 0\\ 0 & 0 & 1\end{bmatrix} \begin{bmatrix}0 & 0 & C_D'-C_L\\ 0 & 0 & C_L'+C_D\\ 0 & 0 & DC_M'\end{bmatrix}\begin{Bmatrix}D\phi_{x,k}\\ D\phi_{y,k}\\ \phi_{\theta,k}\end{Bmatrix}\chi_k(t)\mathrm{d}z \tag{12}$$

The modal mass and modal stiffness corresponding to the mode j are:

$$m_j = \int_0^h \left[D\phi_{x,j}\ D\phi_{y,j}\ \phi_{\theta,j}\right]\mathbf{M}\begin{Bmatrix}D\phi_{x,j}\\ D\phi_{y,j}\\ \phi_{\theta,j}\end{Bmatrix}\mathrm{d}z \tag{13}$$

$$s_j = \int_0^h \left[D\phi_{x,j}\ D\phi_{y,j}\ \phi_{\theta,j}\right]\mathbf{K}\begin{Bmatrix}D\phi_{x,j}\\ D\phi_{y,j}\\ \phi_{\theta,j}\end{Bmatrix}\mathrm{d}z \tag{14}$$

Combining all the above forces, the generalized dynamic equation governing the building motion of mode j becomes:

$$m_j\ddot{\chi} + 4\xi_j m_j\pi n_j\dot{\chi} + m_j 4\pi^2 n_j^2\chi = F_q^j + F_a^j + F_s^j \tag{15}$$

in which n_j is the building's jth natural frequency and ξ_j the structural modal damping ratio.

As previously mentioned, dimensionless equations are obtained after defining dimensionless time and dimensionless frequency as ($\tau = \frac{Ut}{D}, f = \frac{Dn}{U}$). The dimensionless Fourier transformation is defined (with ι imaginary unit) as

$$\hat{\chi}(f) = \int_0^\infty \chi(\tau)e^{-\iota 2\pi f\tau}\mathrm{d}\tau \tag{16a}$$

$$\hat{\dot{\chi}}(f) = \iota 2\pi f\hat{\chi}(f) \tag{16b}$$

$$\hat{\ddot{\chi}}(f) = -4\pi^2 f^2\hat{\chi}(f) \tag{16c}$$

Even though dimensionless Fourier transform has been used for bridge aerodynamics (Scanlan and Jones, 1990), the advantages related to this dimensionless transformation are uncommon and have not been fully exploited in the case of tall buildings. After the dimensionless Fourier transformation, Eq. (15) becomes

$$4\pi^2 m_j\frac{U^2}{D^2}\hat{\chi}_j(f)\left(-f^2 + 2\xi_j f_j\iota f + f_j^2\right) = \hat{F}_q^j(f) + \hat{F}_a^j(f) + \hat{F}_s^j(f) \tag{17}$$

In Eq. (17), the generalized force can be simplified further as:

$$\hat{F}_q^j(f) = \frac{1}{2}\rho D^2U^2 h q_j(f) \tag{18a}$$

$$\hat{F}_a^j(f) = -\iota f\frac{1}{2}\rho D^2U^2 h\sum_{k=1}^{N} c_{j,k}\hat{\chi}_k(f) \tag{18b}$$

$$\hat{F}_s^j(f) = -\frac{1}{2}\rho D^2U^2 h\sum_{k=1}^{N} s_{j,k}\hat{\chi}_k(f) \tag{18c}$$

in which q_j is the dimensionless quasi-steady force for jth mode, $c_{j,k}$ is the dimensionless aerodynamic force and $s_{j,k}$ is the dimensionless aerodynamic stiffness force.

$$q_j = \int_0^1 \Delta(\zeta) \begin{bmatrix} \phi_{x,j} & \phi_{y,j} & \phi_{\theta,j} \end{bmatrix} \begin{bmatrix} \cos\Psi & -\sin\Psi & 0 \\ \sin\Psi & \cos\Psi & 0 \\ 0 & 0 & 1 \end{bmatrix} \begin{bmatrix} 2C_D(\Psi) & C_D'(\Psi) - C_L(\Psi) \\ 2C_L(\Psi) & C_L'(\Psi) + C_D(\Psi) \\ 2C_M(\Psi) & C_M'(\Psi) \end{bmatrix} \begin{Bmatrix} \hat{\mu}(\zeta, f) \\ \hat{v}(\zeta, f) \end{Bmatrix} \mathrm{d}\zeta \tag{19}$$

$$c_{j,k} = \int_0^1 \Delta(\zeta) \begin{bmatrix} \phi_{x,j} & \phi_{y,j} & \phi_{\theta,j} \end{bmatrix} \begin{bmatrix} \cos\Psi & -\sin\Psi & 0 \\ \sin\Psi & \cos\Psi & 0 \\ 0 & 0 & 1 \end{bmatrix} \left[\begin{Bmatrix} 2C_D \\ 2C_L \\ 2C_M \end{Bmatrix} \begin{bmatrix} \cos\Psi & \sin\Psi & 0 \end{bmatrix} + \begin{Bmatrix} C_D' - C_L \\ C_L' + C_D \\ C_M' \end{Bmatrix} \begin{bmatrix} -\sin\Psi & \cos\Psi & 0 \end{bmatrix} \right] \begin{Bmatrix} \phi_{x,k} \\ \phi_{y,k} \\ \phi_{\theta,k} \end{Bmatrix} \mathrm{d}\zeta \tag{20}$$

$$s_{j,k} = \int_0^1 \Delta^2(\zeta) \begin{bmatrix} \phi_{x,j} & \phi_{y,j} & \phi_{\theta,j} \end{bmatrix} \begin{bmatrix} \cos\Psi & -\sin\Psi & 0 \\ \sin\Psi & \cos\Psi & 0 \\ 0 & 0 & 1 \end{bmatrix} \begin{bmatrix} 0 & 0 & C_D' - C_L \\ 0 & 0 & C_L' + C_D \\ 0 & 0 & C_M' \end{bmatrix} \begin{Bmatrix} \phi_{x,k} \\ \phi_{y,k} \\ \phi_{\theta,k} \end{Bmatrix} \mathrm{d}\zeta \tag{21}$$

In the previous equations the quantity ζ is a dimensionless vertical coordinate with $z = \zeta h$, and $\mu = u/U$ and $v = v/U$ is the dimensionless turbulence.

In a classical structural dynamic system, because of mode shape orthogonality, the generalized motion is independent among various modes as along as the structural damping is classical and mode-orthogonal. However, in Eqs. (20) and (21), the aerodynamic damping and stiffness are not necessarily orthogonal to the structural mode shapes. In other words, for the tall buildings with unconventional mode shape, the generalized motion among different modes is coupled due to effects of aerodynamic damping $c_{j,k} \neq 0$ and aerodynamic stiffness $s_{j,k} \neq 0$.

After all substitutions, the generic generalized dynamic modal equation becomes:

$$\left\{ s_{j,j} + \imath f c_{j,j} + \frac{8 m_j \pi^2}{\rho D^4 h} \left[f_j^2 + 2\xi_j f_j \imath f - f_j^2 \right] \right\} \hat{\chi}_j(f) + \sum_{k=1, k\neq j}^{N} \left[s_{j,k} + \imath f c_{j,k} \right] \hat{\chi}_k(f) = q_j \tag{22}$$

2.2. Dimensionless power spectral density of the generalized building force

Because the aerodynamic quasi-steady force is independent of the structural motion, the derivation of the force PSD is straightforward, as indicated by the traditional random vibration approach (Simiu and Scanlan, 1996).

From Eq. (19), the complete generalized force vector for all generalized modal forces is:

$$\mathbf{Q} = \int_0^1 \Delta(\zeta)\, \mathbf{\Phi}(\zeta) \mathbf{C}^{\star} \begin{Bmatrix} \hat{\mu}(\zeta, f) \\ \hat{v}(\zeta, f) \end{Bmatrix} \mathrm{d}\zeta \tag{23}$$

in which the matrix equation of the mode shapes, evaluated at coordinate z or ζ, is:

$$\mathbf{\Phi}(\zeta) = \begin{bmatrix} \phi_{x,1} & \phi_{y,1} & \phi_{\theta,1} \\ \phi_{x,2} & \phi_{y,2} & \phi_{\theta,2} \\ & \cdots & \\ \phi_{x,j} & \phi_{y,j} & \phi_{\theta,j} \\ & \cdots & \\ \phi_{x,N} & \phi_{y,N} & \phi_{\theta,N} \end{bmatrix} \tag{24}$$

It must be noted that there is a slight difference between the $\Phi(\zeta)$ and the original structural mode shape matrix defined in Eq. (4). The building width D has been accounted for in the dimensionless transformation, which is shown in Eq. (18). The original structural mode shape matrix can be re-constructed as $\Phi(\zeta)\mathrm{diag}\begin{bmatrix}D & D & 1\end{bmatrix}$.

$$\mathbf{C}^{\star}=\begin{bmatrix}\cos\Psi & -\sin\Psi & 0\\ \sin\Psi & \cos\Psi & 0\\ 0 & 0 & 1\end{bmatrix}\begin{bmatrix}2C_D(\Psi) & C_D'(\Psi)-C_L(\Psi)\\ 2C_L(\Psi) & C_L'(\Psi)+C_D(\Psi)\\ 2C_M(\Psi) & C_M'(\Psi)\end{bmatrix} \tag{25}$$

Following Davenport Chain in Fig. 1, the PSD of wind force can be derived from the PSD of wind turbulence. In the dimensionless form, the PSD of the generalized force vector is

$$\mathbf{S_{QQ}}=\int_0^1\int_0^1 \Delta(\zeta_1)\Phi(\zeta_1)\mathbf{C}^{\star}\begin{bmatrix}S_{\mu\mu}(\zeta_1,\zeta_2) & \\ & S_{\nu\nu}(\zeta_1,\zeta_2)\end{bmatrix}\mathbf{C}^{\star,T}\mathbf{\Phi}^T(\zeta_2)\Delta(\zeta_2)\mathrm{d}\zeta_1\mathrm{d}\zeta_2 \tag{26}$$

It should be noted that in Eq. (26), the cross-spectrum of along-wind and cross-wind turbulence is ignored for simplicity (Simiu and Scanlan, 1996). Through the above equation, the spectrum of two-directional horizontal turbulence is transformed to the N dimensional generalized force spectrum matrix.

In a single degree-of-freedom system, the transfer function is needed to calculate the structural response spectrum from the generalized force spectrum. For the regular multi degree-of-freedom structural dynamic problem, the motion can be decoupled into several independent modes. Therefore in the frequency domain analysis, the multi degree-of-freedom system can be treated similarly as the single degree-of-freedom one. However, the wind-induced response of a tall building may be affected by unconventional mode shape functions, which may affect the dynamic coupling and, consequently, the mechanism of fluid–structure interaction. As a result, a new unifying (universal) formula is proposed to include these coupling effects through appropriate "aerodynamic damping" and "aerodynamic stiffness" terms.

The dimensionless force vector $\mathbf{Q}$ and response vector $\mathbf{X}$ are defined as:

$$\mathbf{Q}=\begin{bmatrix}q_1 & q_2 & \cdots & q_N\end{bmatrix}^T \tag{27a}$$

$$\mathbf{X}=\begin{bmatrix}\chi_1 & \chi_2 & \cdots & \chi_N\end{bmatrix}^T \tag{27b}$$

$$\mathbf{X}=\mathbf{HQ} \tag{27c}$$

Similar to the single degree-of-freedom generalized problem, the transfer functions matrix $\mathbf{H}$ is needed to link force vector $\mathbf{Q}$ to response vector $\mathbf{X}$. According to Eq. (22), the generic generalized dynamic modal equation of the various modes can be reassembled into the transfer function matrix $\mathbf{H}$.

$$\mathbf{H}=\begin{bmatrix}\hbar_{11} & \hbar_{12} & \dots & \hbar_{1N}\\ \hbar_{21} & \hbar_{22} & \dots & \hbar_{2N}\\ \vdots & \vdots & \ddots & \vdots\\ \hbar_{N1} & \hbar_{N2} & \dots & \hbar_{NN}\end{bmatrix}^{-1} \tag{28a}$$

$$\hbar_{jk}=\begin{cases}s_{j,j}+\imath fc_{j,j}+\dfrac{8m_j\pi^2}{\rho D^4 h}\left[-f^2+2\xi_j f_j\imath f+f_j^2\right] & \text{for } j=k\\ s_{j,k}+\imath fc_{j,k} & \text{for } j\neq k\end{cases} \tag{28b}$$

The PSD of the structural response $\mathbf{S_{XX}}$:

$$\mathbf{S_{XX}}=\mathbf{H}\mathbf{S_{QQ}}\mathbf{H}^{*,T} \tag{29}$$

$\mathbf{H}^{*,T}$ is the conjugate transpose of $\mathbf{H}$.

Since the PSD of generalized response is based on dimensionless time and dimensionless frequency, the variance/covariance matrix of the generalized deformation vector can be directly computed from the integral of $\mathbf{S_{XX}}$ over the dimensionless frequency.

$$\mathbf{\Sigma}(\mathbf{X})=\int_0^{\infty}\mathbf{S_{XX}}\mathrm{d}f \tag{30}$$

Finally, the deformation in generalized modal coordinates can be transformed back to the original physical coordinate system:

$$\Sigma(d(\zeta h))=\begin{bmatrix}D & & \\ & D & \\ & & 1\end{bmatrix}\mathbf{\Phi}^T(\zeta)\mathbf{\Sigma}(\mathbf{X})\mathbf{\Phi}(\zeta)\begin{bmatrix}D & & \\ & D & \\ & & 1\end{bmatrix} \tag{31}$$

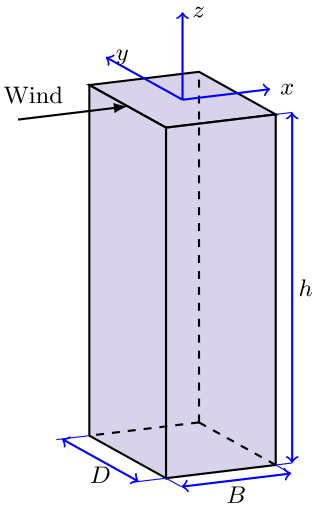

Fig. 3. Schematic view of the *CAARC* benchmark building.

Table 1
3D motion coordinates and wind–pressure force vector representation.

(a) Structural parameters		(b) Wind field parameters	
Quantity	Value assigned	Quantity	Value assigned
B	30.5 m	ρ	1.25 kg/m^3
D	45.7 m	Roughness z_0	0.5 m
h	183 m	$U = U(h)$	0–50 m/s
$m(z)$	223224.4 kg/m	$U(z)$ [m/s]	$U(z/h)^{0.28}$
$\zeta_{s,x}$	0.01	u^*	$U/\left(2.5\ln\frac{h}{z_0}\right)$
$n_{0,x} = n_{0,y} = n_0$ [Hz]	0.2	I_u	$0.53/\left(\ln\frac{h}{z_0}\right)$
$\phi_x(z), \phi_y(z), \phi_z(z)$	$(z/h)^\gamma$; $\gamma = 1$	C_{zu}	12
C_D	1.54	C_{zv}	$0.667C_{zu}$
C_L	0		
$\partial C_L/\partial\Psi$	−3.50		

in which d is the deformation vector in the Cartesian coordinates:

$$d(z) = \begin{bmatrix} x(z) & y(z) & \theta(z) \end{bmatrix}^T \tag{32}$$

3. Numerical verification of the proposed 3D formulation

3.1. Problem statement and description of the simulated structure

In this section, the benchmark tall building of the Commonwealth Advisory Aeronautical Research Council (*CAARC*) (Melbourne, 1980) is selected as the prototype application of the proposed methodology. This building has been widely used in wind engineering as a standard structure for comparison among wind tunnel data and analysis techniques. Fig. 3 illustrates a schematic view of the *CAARC* building with an indication of the main dimensions (depth D, width B, height h).

This building is a slender prismatic structure with a rectangular floor plan, which is symmetric in both primary lateral deformation planes (axes of bending). The mass is distributed uniformly along the building. Table 1a and b summarize the *CAARC* building full-scale properties and the corresponding wind field parameters that are employed in this study. Even though the power law is used to characterize the boundary layer profile (through $\Delta(z)$ or $\Delta(\zeta)$), roughness length is still used to determine turbulence intensities and friction velocity. The mean wind speed direction is orthogonal to the vertical face of dimension D in this section. There are only two modes considered in this validation. The first mode exclusively considers the deformation in the along-wind direction, and the second modes exclusively considers the deformation in the cross-wind direction. High-order modes and torsional modes are ignored in this validation (Piccardo and Solari, 1998b). In summary,

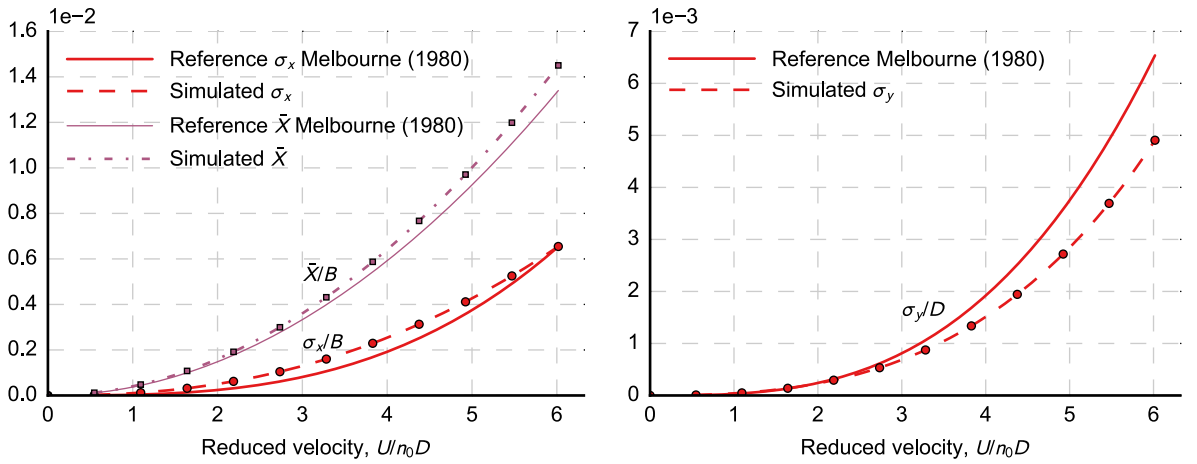

(a) Along-wind response.

(b) Cross-wind response.

Fig. 4. Comparison between simulated response at the roof-top of the *CAARC* building and wind tunnel test results. *Source:* reproduced from Melbourne (1980).

the mode shape matrix function is:

$$\Phi(\zeta) = \begin{bmatrix} \zeta & & \\ & \zeta & \\ & & 0 \end{bmatrix} \tag{33}$$

Fig. 4 illustrates the results obtained for the *CAARC* benchmark building at mean-wind incidence angle $\Psi = 0$. The RMS (root mean square) and mean response ($\bar{X}$) in the along-wind and cross-wind directions, found by the above-described formulation, are compared to wind tunnel results in Melbourne (1980).

Satisfactory correspondence between the numerical results and the reference data, reproduced from Melbourne (1980), can be observed, with the largest discrepancies noticeable in the cross-wind response (about 25% difference at reduced velocity $U/n_0D = 6$). This result was anticipated as a result of the quasi-steady approximation, which does not account for wake-induced loading (vortex shedding). This aspect will be considered in Section 4. Despite the symmetry of the *CAARC* building and the assumption on uni-planar lateral mode shapes, this example confirms the validity of the proposed formulation for this particular geometry. More investigation is needed to adequately examine the validity of the proposed formulation in the case of more complex building geometry; further validation was also not possible due to inherent limitations in the experimental setup (Section 4), pointed out in previous studies (Cui and Caracoglia, 2016, 2017). This aspect will be investigated in future studies.

3.2. Examination of the coupled 3D formulation through numerical examples

In order to comprehensively investigate the structural response of the *CAARC* building at any generic mean-wind incidence angle, rather than at fixed direction $\Psi = 0$ or $\Psi = \pi/2$ (90°), several numerical examples with various assumptions and mode shape functions are considered in this section.

Since wind directions are not limited to any specific orientation, the aerodynamic coefficients should be continuous functions of the wind direction Ψ. The geometry of the tall building analyzed in this section still corresponds to the *CAARC* building, used in the previous section. The aerodynamic coefficients, $C_D(\Psi)$, $C_L(\Psi)$ and $C_M(\Psi)$, as well as their derivatives with respect to Ψ are found from Fig. 5; the data are derived from a wind tunnel test conducted at Northeastern University (NEU) on a 1:750-scale rigid model of this building. Details are described in Cui and Caracoglia (2016, 2017). Both experimental data points and fitting curves are displayed in the figure. Some differences must be noted between the results in Fig. 5 and the values in Table 1a. As briefly outlined in the previous section, one of the reasons can be related to the experimental setup available at Northeastern University and its limitations (Cui and Caracoglia, 2016), which led to some simplifications in the replication of the boundary layer flow in the NEU's laboratory. In the context of this study, differences are however acceptable.

In the first study case, the first three fundamental modes are considered. The structural mode shapes are fully independent (i.e. absence of coupling between torsion and lateral translation in the mode shapes). More specifically, the first-mode shape only pertains to lateral-translation motion in the x direction; the second and third modes only contain translation along the y direction and rotation about z axis, respectively. Therefore, the dimensionless mode shape matrix function is postulated

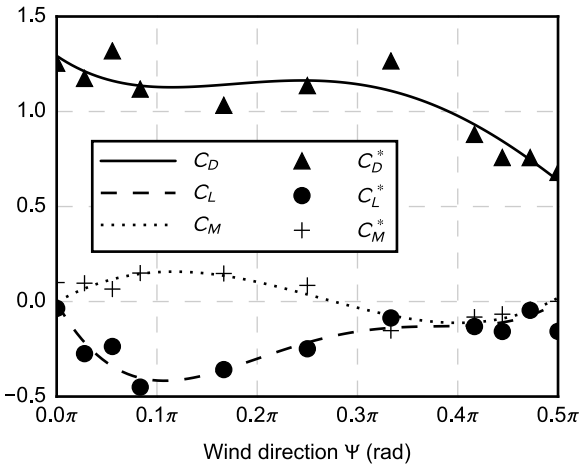

Fig. 5. Variation of the *CAARC's* aerodynamic force coefficients per unit height C_D, C_L and C_M with mean wind direction Ψ (notes: discrete points with various markers are the experimental data C_D^*, C_L^* and C_M^*; continuous lines are the fitted curves by Fourier series).

as:

$$\Phi(\zeta) = \begin{bmatrix} 1 & 0 & 0 \\ 0 & 1 & 0 \\ 0 & 0 & 1 \end{bmatrix} \zeta \tag{34}$$

The first- and second-mode natural frequencies are reported in Table 1a; the third (torsional mode) natural frequency is assumed as 0.4 Hz.

From basic random vibration theory, the variances of the structural motion can be derived from the PSD functions. For example, the structural motion in the x direction at the reference elevation (building roof-top) is: $\sigma_x^2 = \int_0^\infty S_{xx}(n)\mathrm{d}n$. If the structural motion is a stationary Gaussian process, which is usually acceptable in the case of single-direction wind-induced structural dynamic analysis, the peak response (or lateral deformation) may be computed as Davenport (1964):

$$x_{\text{peak}} = x_{\text{mean}} + \left[(2 \ln \nu_x T)^{1/2} + \frac{0.577}{(2 \ln \nu_x T)^{1/2}} \right] \sigma_x \tag{35}$$

where $\nu_x = \left(\int_0^\infty n^2 S_{xx}(n)\mathrm{d}n / \int_0^\infty S_{xx}(n)\mathrm{d}n \right)^{1/2}$, and T is the duration of the observation interval, which is usually taken as 600 s (mean-wind averaging time).

However, when conducting a structural performance analysis the resultant wind-induced response should take into account along-wind, cross-wind and torsional response simultaneously. As a result, the structural response process is non-Gaussian, and the method described in Eq. (35) is only approximate. In this study, a numerical approach based on the translation process theory and inspired by theoretical developments in Chen and Huang (2009) is used to estimate the peak resultant response; more detailed description of this approach may be found in Cui and Caracoglia (2015). The peak resultant response at various mean wind speeds (referenced at the building roof-top) and wind directions is presented in Fig. 6(a).

Fig. 6(a) suggests that the maximum structural deformation at the buidling roof-top is observed at neither $\Psi = 0$ nor $\Psi = \pi/2$ (90°). At $\Psi \approx 0.30\pi$ (55°), the largest lateral deflection is found for almost all wind speeds. In contrast, lateral roof-top deflections are approximately 14% smaller at $\Psi = 0$.

The second case study, presented in Fig. 6(b), examines structural coupling and 3D mode shapes with:

$$\Phi(\zeta) = \begin{bmatrix} 1 & 0 & 0.04 \\ 0 & 1 & 0 \\ 0.01 & 0 & 1 \end{bmatrix} \zeta \tag{36}$$

In the first and third mode, the structural motion is coupled between the x and z directions. Similar to the previous case, the maximum peak displacement is determined when the mean wind direction is around 0.30π (55°).

Fig. 7 presents the peak torsional response (floor rotation at the building roof-top) for the two above-described cases.

With uncoupled mode shapes, the torsional motion is very small and the amplitude of the torsional response is less than 10^{-5} rad, negligible in comparison with the lateral translation results in Fig. 6. This outcome is expected since the wind-induced torque is relatively unimportant for such a symmetric building shape (Melbourne, 1980). Nevertheless, when the mode shapes are coupled as in Eq. (36), the torsional rotation is excited owing to the coupling and the effects of the along-wind force. Consequently, contrary to the lateral translation motion, the torsional motion is maximum at $\Psi = 0$, and

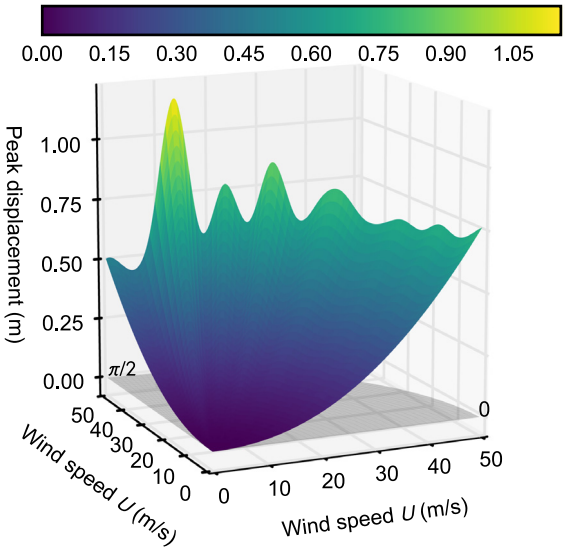

(a) Uncoupled mode shapes.

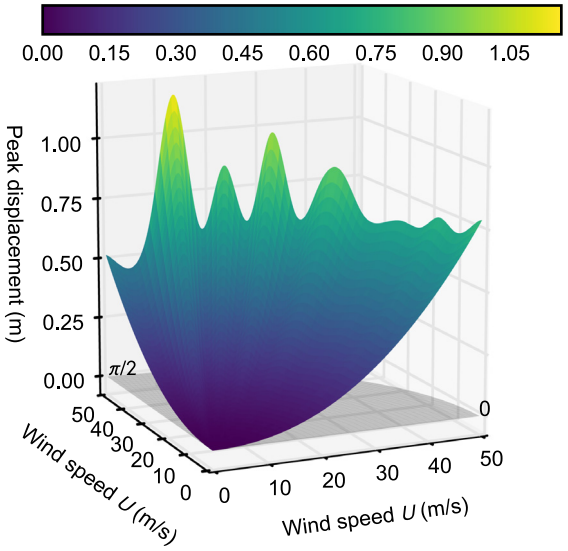

(b) 3D coupled mode shapes.

Fig. 6. Peak resultant lateral roof-top response of the *CAARC* building for various mean wind speeds U and directions Ψ (note: a different brightness in the colorbar is used to designate various deformation amplitudes).

its magnitude is drastically magnified by about 100 times. In other words, the coupled mode shapes will greatly influence the wind-induced building response even though the building shape and aerodynamics are the same.

In the last example, the approach is adapted to study a structure with 3D coupled modes and nonlinear mode shape functions. The parabolic mode shape functions, describing the first two lateral modes and torsional mode, are presented in the matrix equation below:

$$\mathbf{\Phi}(\zeta) = \begin{bmatrix} 1 & 0 & 0.04 \\ 0 & 1 & 0 \\ 0.01 & 0 & 1 \end{bmatrix} \zeta^2 \tag{37}$$

Fig. 8 illustrates the roof-top peak translation and peak torsional angle at various reference mean wind speeds and directions with coupled nonlinear mode shapes [Eq. (37)]. In comparison with Figs. 6(b) and Fig. 7(b), the overall trends are similar but the response magnitude increases by about 25% on average. Aerodynamic forces at higher floors (larger z)

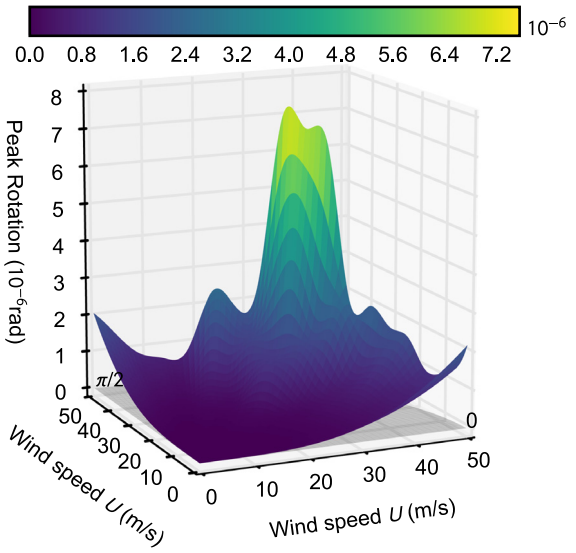

(a) Uncoupled mode shapes.

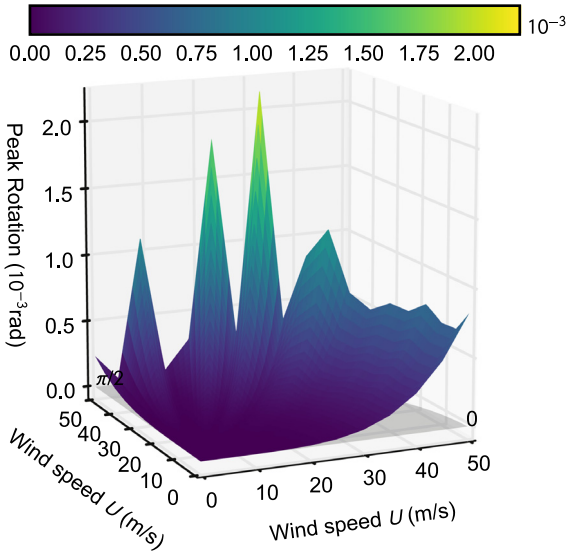

(b) 3D coupled mode shapes.

Fig. 7. Peak torsional response at the roof-top of the *CAARC* building at various reference mean wind speeds U and directions Ψ (note: a different brightness in the colorbar is used to designate various rotation amplitudes).

have a greater dynamic effect on the structural response because of the relatively larger modal deformations, exacerbated by the parabolic mode shapes.

4. Preliminary experimental validation, incorporating wake-induced load effects within the proposed 3D formulation

4.1. Theoretical background

The High Frequency Force Balance (HFFB) is an experimental method for the estimation of the generalized aerodynamic force from the time series of wind forces measured in wind tunnel (e.g., Bernardini et al., 2012). In comparison with the quasi-steady method described in the previous section, the HFFB method has two advantages: (1) the HFFB test result evaluates the full wind load and includes vortex-shedding effects, which the quasi-steady theory cannot simulate;

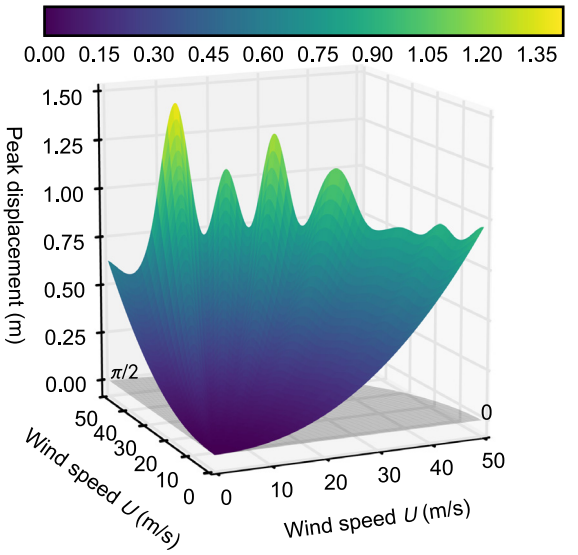

(a) Lateral response.

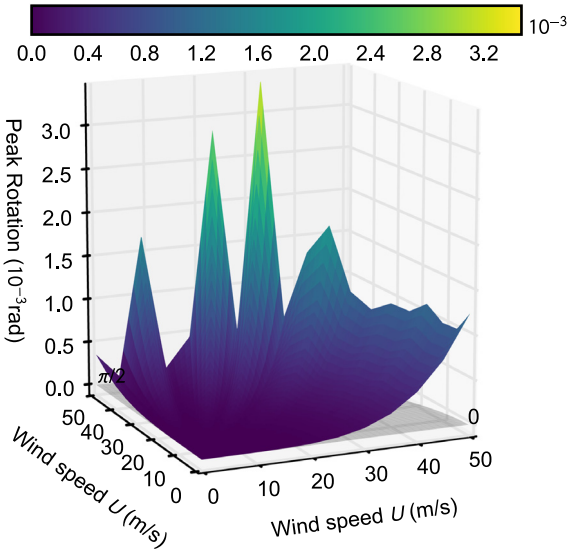

(b) Torsional response.

Fig. 8. Peak resultant roof-top lateral response and torsional response of the *CAARC* building with 3D coupled modes and nonlinear mode shape functions.

(2) the HFFB method can avoid the calculation of the double integral in Eq. (26), which usually requires large computing resources (Smith and Caracoglia, 2011). Using the HFFB test and eliminating the calculation of the $\mathbf{S_{QQ}}$ can significantly reduce the computing time. However, the limitation of HFFB results is that the lateral mode shape functions must be linear along the height so that the base bending moment can directly be used as the generalized modal force. For structures with nonlinear mode shapes, the HFFB may still be utilized after appropriate correction, such as the method in Zhou et al. (2002) or in Holmes (1987).

In this study, all the generalized forces need to be unified using the same normalization. Due to the formula and the derivation in Eq. (18), the same force normalization is used: $1/2\rho U^2 D^2 h$ for along-wind force, cross-wind force and torque.

Because of the definition of the HFFB method in Davenport and Tschanz (1981), the PSD results can only be used with linear structural mode shapes along the three main deformation planes following $\mathbf{S_{Q_jQ_l}}$ in Eq. (38)

$$\mathbf{S_{Q_jQ_l}} = \iint_0^1 \Delta(\zeta_1)\mathbf{\Phi}_l(\zeta_1)\mathbf{C}^{\star}\begin{bmatrix} S_{\mu\mu}(\zeta_1,\zeta_2) & \\ & S_{\nu\nu}(\zeta_1,\zeta_2) \end{bmatrix}\mathbf{C}^{\star,T}\mathbf{\Phi}_l^T(\zeta_2)\Delta(\zeta_2)\mathrm{d}\zeta_1\mathrm{d}\zeta_2 \tag{38}$$

The quantity $\mathbf{S}_{\mathbf{Q}_l\mathbf{Q}_l}$ is the generalized force PSD with three uncoupled linear mode shapes as:

$$\Phi_l(\zeta) = \begin{bmatrix} 1 & 0 & 0 \\ 0 & 1 & 0 \\ 0 & 0 & 1 \end{bmatrix} \zeta \tag{39}$$

For building structures with unconventional mode shape functions, a modification to $\Phi_l(\zeta)$ is necessary to use the HFFB results with the structural response analysis.

$$\mathbf{S}_{\mathbf{QQ}} = \mathbf{\Lambda}\mathbf{\Xi}\mathbf{S}_{\mathbf{Q}_l\mathbf{Q}_l}\mathbf{\Xi}^T\mathbf{\Lambda}^T \tag{40a}$$

$$\mathbf{\Lambda} = \begin{bmatrix} \lambda_1 & \lambda_2 & \cdots & \lambda_N \end{bmatrix}^T \tag{40b}$$

$$\boldsymbol{\lambda}_j = \begin{bmatrix} p_{1j}\beta_{1j} & p_{2j}\beta_{2j} & p_{3j}\beta_{3j} \end{bmatrix} \tag{40c}$$

$$\mathbf{\Xi} = \begin{bmatrix} \cos\Psi & -\sin\Psi & 0 \\ \sin\Psi & \cos\Psi & 0 \\ 0 & 0 & 1 \end{bmatrix} \tag{40d}$$

In the previous equations, $\mathbf{\Lambda}$ is a modification matrix constructed using N modification vectors λ_j for each mode in accordance with the procedure described in Zhou et al. (2002). In each λ_j, p_{1j}, p_{1j} and p_{2j} are the components of the jth mode shape in the three directions or planes (so, at least one of p_{1j}, p_{1j} and p_{2j} is equal to 1); β_{1j}, β_{2j} and β_{3j} are the nonlinear mode shape correction factors (Zhou et al., 2002). Details are not presented herein but may be found in Zhou et al. (2002). The quantity $\mathbf{\Xi}$ is the coordinate transformation matrix that transfers the generalized force matrix, experimentally estimated according to the global coordinates (along-wind and cross-wind), to the structure's x–y local coordinate system. After modification and coordinate transformation, the HFFB force spectrum can be used as the input for the generalized modal force spectrum. Consequently, the structural response will be calculated from the HFFB results as shown in Eq. (29).

4.2. Numerical application example

This sub-section provides an example to demonstrate the capability of the theoretical formulation, combined with the HFFB experimental force estimation.

The HFFB data are reproduced from an experiment, conducted in the NEU's small-scale wind tunnel. Due to the limitation of the experimental equipment, replication of a boundary layer flow was not possible; consequently, a homogeneous turbulence flow with a constant vertical profile mean profile can exclusively be reproduced in the wind tunnel (Cui and Caracoglia, 2016). A previous study (Cui and Caracoglia, 2016) has shown that the generalized along-wind and cross-wind forces (i.e. the first two diagonal terms of the $\mathbf{S}_{\mathbf{Q}_l\mathbf{Q}_l}$ matrix) found from HFFB test results carried out on the CAARC model in the NEU's wind tunnel approximately match the original HFFB results by Saunders and Melbourne (1975): the dominant cross-wind spectrum peak at $\Psi = 0$ in correspondence with the shedding frequency is correctly reproduced (around 0.11 in dimensionless units) and the magnitudes of the spectrum are compatible. Even though some discrepancies were noticed [as explained in detail in the previous study (Cui and Caracoglia, 2016)] the NEU's experimental results are acceptable for the purposes of this investigation and are employed in the remainder of this section for validation. Nevertheless, a more accurate wind tunnel experiment using a model with more complex building geometry is possibly needed in the future to enable supplementary investigations.

In order to replicate the features of the homogeneous turbulence wind flow with constant mean wind speed along z, the flow parameters are configured to the homogeneous wind flow by setting the exponent of the power-law boundary layer profile equal to 0 (i.e. $U(z) = U(h) = U$). Using the HFFB-based experimental generalized loads, the largest deformations occurs at $\Psi = 0$ mean-wind incidence angle as a consequence of the strong vortex-shedding effects, which are most significant for this rectangular floor-plan building when the wind direction is perpendicular to the vertical face D. On the contrary, using the theoretical quasi-steady aerodynamic loads results in the largest deformation at about $\Psi = 0.30\pi$ (55°) as discussed in Section 3.2. Moreover, the results in Fig. 9 suggest that the response found by HFFB-based experimental generalized loads is considerably larger than the one determined by theoretical quasi-steady aerodynamic method. This discrepancy is possibly related to two main reasons: (1) the HFFB-based wind forces include vortex-shedding effects; (2) the spatial turbulence correlation of the NEU's homogeneous wind field is much stronger (along the z direction) than the theoretical model, which assumes a decay factor $C_{zu} = 12$ in the coherence function. In any case, this example demonstrates that the proposed unified formulation, introduced in this study, can successfully be adapted to incorporate HFFB-based experimental results in the analysis of a tall building response.

5. Conclusions

This study examines the well-known quasi-steady theory, widely applied in wind engineering, and derives a novel generalized aerodynamic formulation in Eq. (22) for evaluating the coupled dynamic response of a tall, slender bluff body. The proposed formulation explores complex structural motion and multi-directional wind load effects by combining aerodynamic damping, aerodynamic stiffness and inter-modal coupling in a "universal formula". Dimensionless dynamic

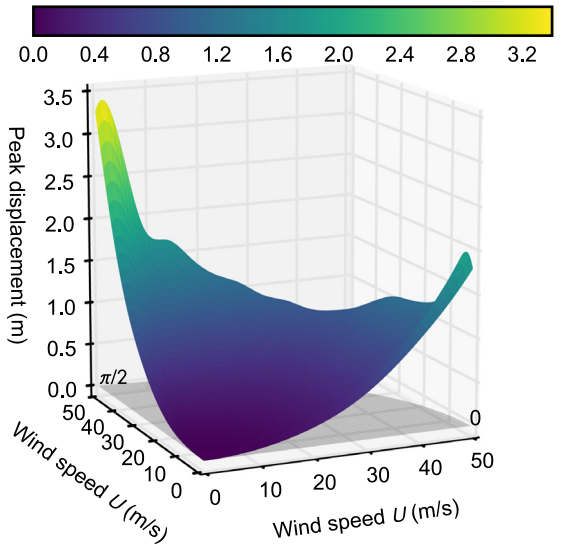

(a) HFFB results.

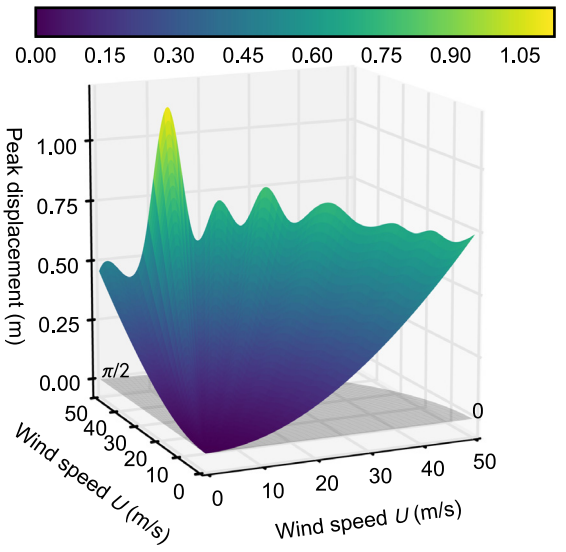

(b) Theoretical quasi-steady results only.

Fig. 9. Comparison of peak resultant roof-top lateral response using HFFB-based experimental generalized forces and theoretical quasi-steady results.

equations and dimensionless Fourier transformation are used to generalize and simplify the format of the formula. In the second part of this study, several numerical examples are provided to examine the peak lateral displacements and peak torsional rotation at various mean wind speeds and mean wind directions on the roof-top of a benchmark building. The examples demonstrate that the theoretical formulation can adequately analyze various building systems with either linear or nonlinear mode shape functions, coupled or uncoupled mode shapes. In addition, the investigation suggests that HFFB experimental results can be incorporated into the theoretical formulation to predict the structural response. As a consequence, the proposed formulation opens a new and efficient way to calculate the wind-induced dynamic response of tall buildings with unconventional structural behavior.

Acknowledgments

This material is based upon work supported in part by the National Science Foundation (NSF) of the United States under CAREER Award CMMI-0844977 in 2009–2014. The partial support of NSF Award CMMI-1434880 is also acknowledged. Any

opinions, findings and conclusions or recommendations are those of the authors and do not necessarily reflect the views of the NSF.

References

Bashor, R., Kareem, A., 2007. Probabilistic performance evaluation of buildings: an occupant comfort perspective. In: Proceedings of the 12th International Conference on Wind Engineering.
Bernardini, E., Spence, S.M., Gioffrè, M., 2012. Effects of the aerodynamic uncertainties in HFFB loading schemes on the response of tall buildings with coupled dynamic modes. Eng. Struct. 42, 329–341.
Chen, X., Huang, G., 2009. Evaluation of peak resultant response for wind-excited tall buildings. Eng. Struct. 31 (4), 858–868.
Chen, X., Kareem, A., 2005. Coupled dynamic analysis and equivalent static wind loads on buildings with three-dimensional modes. J. Struct. Eng. 131 (7), 1071–1082.
Chuang, W., Spence, S., 2017. A performance-based design framework for the integrated collapse and non-collapse assessment of wind excited buildings. Eng. Struct. 150, 746–758.
Ciampoli, M., Petrini, F., 2012. Performance-based aeolian risk assessment and reduction for tall buildings. Probab. Eng. Mech. 28, 75–84.
Ciampoli, M., Petrini, F., Augusti, G., 2011. Performance-based wind engineering: Towards a general procedure. Struct. Saf. 33 (6), 367–378.
Cui, W., Caracoglia, L., 2015. Simulation and analysis of intervention costs due to wind-induced damage on tall buildings. Eng. Struct. 87, 183–197.
Cui, W., Caracoglia, L., 2016. Physics-based method for the removal of spurious resonant frequencies in high-frequency force balance tests. J. Struct. Eng. 142 (2), 04015129.
Cui, W., Caracoglia, L., 2017. Examination of experimental variability in HFFB testing of a tall building under multi-directional winds. J. Wind Eng. Ind. Aerodyn. 171 (0), 34–49.
Davenport, A.G., 1961. A Statistical Approach to the Treatment of Wind Loading on Tall Masts and Suspension Bridges (Ph.D. dissertation). University of Bristol, United Kingdom.
Davenport, A.G., 1964. Note on the distribution of the largest value of a random function with application to gust loading. In: ICE Proceedings. Thomas Telford, pp. 187–196.
Davenport, A.G., Tschanz, T., T981. The response of tall buildings to wind. In: Proceedings of the Fourth US National Conference of Wind Engineering, Seattle, Washington, USA.
Ellingwood, B., Rosowsky, D., Li, Y., Kim, J., 2004. Fragility assessment of light-frame wood construction subjected to wind and earthquake hazards. J. Struct. Eng. 130 (12), 1921–1930.
Ellingwood, B., Tekie, P., 1999. Wind load statistics for probability-based structural design. J. Struct. Eng. 125 (4), 453–463.
Hart, G.C., Jain, A., 2013. Performance based wind design of tall concrete buildings in the Los Angeles region utilizing structural reliability and nonlinear time History analysis. In: The 12th Americas Conference on Wind Engineering, 12ACWE.
He, M., Macdonald, J.H., 2016. An analytical solution for the galloping stability of a 3 degree-of-freedom system based on quasi-steady theory. J. Fluids Struct. 60, 23–36.
Holmes, J., 1987. Mode shape corrections for dynamic response to wind. Eng. Struct. 9 (3), 210–212.
Inokuma, A., 2002. Basic study of performance-based design in civil engineering. J. Profess. Iss. Eng. Educ. Pract. 128 (1), 30–35.
Isyumov, N., 2012. Alan G. Davenport's mark on wind engineering. J. Wind Eng. Ind. Aerodyn. 104, 12–24.
Jain, A., Srinivasan, M., Hart, G.C., 2001. Performance based design extreme wind loads on a tall building. Struct. Des. Tall Build. 10 (1), 9–26.
Kareem, A., 1985. Lateral-torsional motion of tall buildings to wind loads. J. Struct. Eng. 111 (11), 2479–2496.
Melbourne, W.H., 1980. Comparison of measurements on the CAARC standard tall building model in simulated model wind flows. J. Wind Eng. Ind. Aerodyn. 6 (1), 73–88.
Nguyen, C.H., Freda, A., Solari, G., Tubino, F., 2015. Aeroelastic instability and wind-excited response of complex lighting poles and antenna masts. Eng. Struct. 85 (Suppl. C), 264–276.
Norton, T., Abdullah, M., Stephens, D., 2008. Proposed methodology for performance-based vulnerability assessment of wind-excited tall buildings. In: Fourth International Conference on Advances in Wind and Structures, AWAS, pp. 1228–1246.
Piccardo, G., Solari, G., 1998a. Closed form prediction of 3-D wind-excited response of slender structures. J. Wind Eng. Ind. Aerodyn. 74, 697–708.
Piccardo, G., Solari, G., 1998b. Generalized equivalent spectrum technique. Wind Struct. 1 (2), 161–174.
Piccardo, G., Solari, G., 2000. 3D wind-excited response of slender structures: Closed-form solution. J. Struct. Eng. 126 (8), 936–943.
Saunders, J., Melbourne, W., 1975. Tall rectangular building response to cross-wind excitation. In: Proc. 4th Int. Conf. on Wind Effects on Buildings and Structures. Cambridge University Press, London, pp. 369–380.
Scanlan, R.H., Jones, N.P., 1990. Aeroelastic analysis of cable-stayed bridges. J. Struct. Eng. 116 (2), 279–297.
SEAOC, 1995. Vision 2000: Performance Based Seismic Engineering of Buildings. Structural Engineers Association of California, Sacramento, California.
Simiu, E., Scanlan, R.H., 1996. Wind Effects on Structures: Fundamentals and Applications to Design, third ed. John Wiley & Sons, New Jersey, USA.
Smith, M.A., Caracoglia, L., 2011. A Monte Carlo based method for the dynamic "fragility analysis" of tall buildings under turbulent wind loading. Eng. Struct. 33 (2), 410–420.
Solari, G., 1993a. Gust buffeting. I: Peak wind velocity and equivalent pressure. J. Struct. Eng. 119 (2), 365–382.
Solari, G., 1993b. Gust buffeting. II: Dynamic alongwind response. J. Struct. Eng. 119 (2), 383–397.
Spence, S.M., Kareem, A., 2014. Performance-based design and optimization of uncertain wind-excited dynamic building systems. Eng. Struct. 78, 133–144.
Zhou, Y., Kareem, A., Gu, M., 2002. Mode shape corrections for wind load effects. J. Eng. Mech. 128 (1), 15–23.